Journal of Physics Communications

PAPER

Visualization of correlations in hybrid discrete–continuous variable quantum systems

R P Rundle[1,2], B I Davies[1], V M Dwyer[1,2], Todd Tilma[1,3,4] and M J Everitt[1]

[1] Quantum Systems Engineering Research Group, Department of Physics, Loughborough University, Leicestershire LE11 3TU, United Kingdom
[2] The Wolfson School, Loughborough University, United Kingdom
[3] Department of Physics, College of Science, Tokyo Institute of Technology, H-63, 2-12-1 Ōokayama, Meguro-ku, Tokyo 152-8550, Japan
[4] Quantum Computing Unit, Institute of Innovative Research, Tokyo Institute of Technology, S1-16, 4259 Nagatsuta-cho, Midori-ku, Yokohama 226-8503, Japan

E-mail: m.j.everitt@physics.org

Keywords: Wigner function, phase space, quantum Mechanics, hybrid Systems, correlations

OPEN ACCESS

RECEIVED
10 October 2019

REVISED
24 January 2020

ACCEPTED FOR PUBLICATION
24 January 2020

PUBLISHED
4 February 2020

Abstract

In this work we construct Wigner functions for hybrid continuous and discrete variable quantum systems. We demonstrate new capabilities in the visualization of the interactions and correlations between discrete and continuous variable quantum systems, where visualizing the full phase space has proven difficult in the past due to the high number of degrees of freedom. Specifically, we show how to clearly distinguish signatures that arise due to quantum and classical correlations in an entangled Bell-cat state. We further show how correlations are manifested in different types of interaction, leading to a deeper understanding of how quantum information is shared between two subsystems. Understanding the nature of the correlations between systems is central to harnessing quantum effects for information processing; the methods presented here reveal the nature of these correlations, allowing a clear visualization of the quantum information present in these hybrid discrete-continuous variable quantum systems. The methods presented here could be viewed as a form of quantum state spectroscopy.

1. Introduction

Quantum correlations have become central to the design and manufacture of various quantum technologies [1–4]. Whether these quantum correlations are found between macroscopically distinct superpositions of states, also known as Schrödinger cat states, or in the entanglement between multiple systems. Currently, such technologies can be broadly categorized as being based on either continuous-variable (CV) or discrete-variable (DV) quantum systems.

For CV systems, the primary focus has been on quantum optical systems; manipulating coherent states of light for various quantum information processing applications [5–8]. In such systems, the Wigner function [9, 10] is commonly used due to its ability to display an intuitive representation of a quantum state. Furthermore, the Wigner function is particularly good at revealing coherences and correlations, such as squeezing and superposition [11]. For these reasons, it has become a fundamental tool in the 'search' for Schrödingers cats [12], readily identified by the iconic interference patterns arising from its quantum correlations.

By contrast the focus for DV systems has been on exploiting two-level quantum systems—*qubits*—in order to generate a quantum analogue of the classical bit [2, 13, 14]. Here, the Wigner function has received little attention as a means of visualization. Unlike the case of CV systems, there are two common approaches for generating informationally complete DV Wigner functions, both of which have found application. The approach developed in [15, 16] uses discrete degrees of freedom and has proven useful for quantum information purposes, particularly in the case of contextuality and Wigner function negativity [17–19]. The second approach (and the one used in this work) uses a DV Wigner function with continuous degrees of freedom, similar to the

Bloch sphere [20–26]. For example, there have been various proposals put forward that use a continuous Wigner function to reveal correlations between DV systems [26–28]. These methods have further been validated through the direct measurement of phase-space to reveal quantum correlations [28–31]. Recently this has been extended to experiments validating atomic Schrödinger cat states of up to 20 superconducting qubits [32].

A case that has not been explored in much detail is the phase-space representation of CV-DV hybridization. This hybridisation is seen in many applications of quantum technologies, including simple gate models for quantum computers, such as hybrid two-qubit gates [33, 34], and CV microwave pulse control of DV qubits [35]. The generation of hybrid quantum correlations within CV-DV hybrid[5] systems commonly takes place within the framework of cavity quantum electrodynamics, that describes the interaction between a two-level quantum system and a single mode of a microwave field. These models can be further used to describe the effect of circuit quantum electrodynamics, and to consider the interaction of the microwave field with an artificial atom. Analyzing these interactions within the framework of the Jaynes–Cummings model [36] allows us to display how quantum information is shared between the CV and DV systems.

A number of papers [23, 24, 37] have shown the mathematical construction of hybrid states within the phase space, these have been constructed without giving a way to visually display the degrees of freedom of such composite systems. A method for displaying states with heterogeneous degrees of freedom, using the Wigner function, came from the application of composite phase-space methods to quantum chemistry [38]. The technique presented here is based on this approach, however in [38], reduced Wigner functions are used and an envelope is further applied, potentially losing many of the non-local correlations that arise due to entanglement. Other methods for combining CV Wigner function tomography with other representations of DV systems have been created [39–41], however, only the CV system was treated using the Wigner function formulation. The visualization technique used in [38] displays heterogeneous degrees of freedom, highlighting the power of a hybrid Wigner function approach for visualizing correlations. This approach also demonstrates how many of the correlations are lost when using standard phase-space methods, such as the reduced Wigner function. A hybrid phase-space representation, of all the information within these hybrid systems, is crucial for a more complete understanding of CV-DV hybridization, and its physical properties [42–44]. This understanding will be especially helpful for advancing quantum technologies [34, 45–48], in particular quantum communication where CV-DV hybridization has been used for teleportation [49–51] and entanglement distillation [52–54].

Using the procedure laid out in [24] to generate any quantum state in phase space, and adapting the visualization method from [38], we show how the Wigner function of a hybrid system can be intuitively represented. We begin by presenting examples of important states for CV and DV systems, illustrating how our representation makes correlation information clear. We extend our analysis using the Jaynes–Cummings model to show how intuitive this representation can be. The results open new directions for the use of phase-space methods in hybrid quantum systems.

2. The Wigner function

The Wigner function is traditionally introduced as the Fourier transform of an autocorrelation function [9, 55]. Here it is more suitable to consider a general Wigner function of some arbitrary operator $\hat{A}$, defined as [56]

$$W_{\hat{A}}(\Omega) = \mathrm{Tr}\left[\hat{A}\ \hat{\Pi}(\Omega)\right], \tag{1}$$

where $\hat{\Pi}(\Omega)$ is the displaced parity operator for some parameterization of phase space Ω. The displaced parity operator is defined through displacing a generalized parity operator [24], and for the CV Wigner function is [57]

$$\hat{\Pi}_f(\alpha) = 2\hat{D}(\alpha)\hat{\Pi}_f\hat{D}^{\dagger}(\alpha), \tag{2}$$

where $\hat{\Pi}_f = \sum_{i=0}^{\infty}(-1)^i|i\rangle\langle i|$, written here as an operator in the Fock basis, is the usual parity operator that reflects a point through the origin and

$$\hat{D}(\alpha) = \exp\left(\alpha\hat{a}^{\dagger} - \alpha^{*}\hat{a}\right) \tag{3}$$

is the standard CV displacement operator written using the annihilation and creation operators, $\hat{a}$ and $\hat{a}^{\dagger}$, respectively. Note that we have introduced the subscript *f*, for 'field', to indicate CV systems. The displacement operator can be used to define a coherent state [57]

$$|\beta\rangle_f = \hat{D}(\beta)|0\rangle_f, \tag{4}$$

as the displacement of the vacuum state, $|0\rangle_f$, generating a new coherent state $|\beta\rangle_f$.

As shown in [23, 24], a similar approach to (2) can be used to generate Wigner functions for arbitrary quantum systems. For two-level DV systems, for example,

[5] From now on, we shall refer to CV-DV hybrid states as simply 'hybrid states', dropping 'CV-DV'.

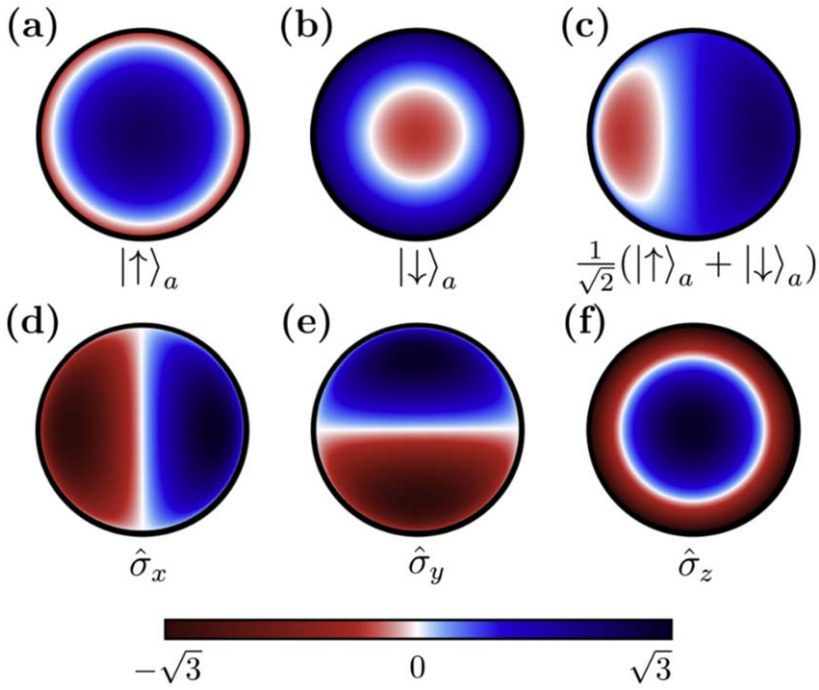

Figure 1. Shown here are six example qubit Wigner functions using the Lambert azimuthal equal-area projection, that maps a sphere onto a circle where the north pole is mapped to the centre and the south pole is on the perimeter. Three single-qubit pure states are shown in (a)–(c), where (a) and (b) are the eigenstates of $\hat{\sigma}_z$, $|\uparrow\rangle_a$ and $|\downarrow\rangle_a$, with eigenvalues ± 1 respectively. (c) is the equal superposition of the states in (a) and (b), $(|\uparrow\rangle_a + |\downarrow\rangle_a)/\sqrt{2}$. (d)–(f) show the qubit Wigner functions of the three Pauli matrices, $\hat{\sigma}_x$, $\hat{\sigma}_y$, and $\hat{\sigma}_z$ respectively.

$$\hat{\Pi}_a(\theta, \phi) = \hat{U}(\theta, \phi, \Phi)\hat{\Pi}_a\hat{U}^{\dagger}(\theta, \phi, \Phi), \tag{5}$$

where the generalized parity, $\hat{\Pi}_a$, for a single, two-level, system is $\hat{\Pi}_a = (\hat{\mathbb{1}} + \sqrt{3}\,\hat{\sigma}_z)/2$ [23, 24, 28], for a full derivation of the kernel see [58]. Note that the subscript a here indicates that this is a state for the 'atom', or DV system. The analogue of the displacement operator, $\hat{U}(\theta, \phi, \Phi)$, given in terms of Euler angles, is

$$\hat{U}(\theta, \phi, \Phi) = \exp(\mathrm{i}\hat{\sigma}_z\phi)\exp(\mathrm{i}\hat{\sigma}_y\theta)\exp(\mathrm{i}\hat{\sigma}_z\Phi) \tag{6}$$

for the standard Pauli matrices $\hat{\sigma}_y$ and $\hat{\sigma}_z$. Note as the parity operator commutes with $\hat{\sigma}_z$, the Φ term does not contribute, and the DV Wigner function depends only on θ and ϕ, allowing it to be plotted on the surface of a sphere. Note that by DV Wigner function, we mean the Wigner function for DV systems; the Wigner function used here is however parameterized over the continuous variables θ and ϕ.

figure 1 shows examples of the DV Wigner function generated by (5) for some simple qubit states. Each of the DV Wigner functions presented in figure 1 is plotted following [59], using the Lambert azimuthal equal-area projection [60]. This projection is area preserving and maps the surface of a sphere to polar coordinates, with the north pole mapped to the centre of the disc and the south pole to the outer boundary. The equator of the sphere is projected onto a concentric circle, with a radius $1/\sqrt{2}$ times the radius of the entire circle, this is explicitly seen as the white circle in figure 1(f). This means that the Lambert azimuthal equal-area projection allows us to view the entire surface of the sphere as a circle. The reason for using this area-preserving mapping, rather than an angle-preserving mapping, is because we are dealing with a probability distribution function. By definition, the integral over a volume determines the probability; area-preserving therefore translates into probability-preserving. A consequence of this mapping is that in some regions of phase space, the quasi-probability distribution appears warped. For instance, the first three states in figures 1(a)–(c) are all rotations of one another on a sphere.

The DV Wigner functions presented in figures 1(a)–(c) are standard two-level quantum states, where figures 1(a) and (b) are the ± 1 eigenstates of the $\hat{\sigma}_z$ operator, $|\uparrow\rangle_a$ and $|\downarrow\rangle_a$ respectively. The state in figure 1(c) is the equal superposition of $|\uparrow\rangle_a$ and $|\downarrow\rangle_a$, or the positive eigenstate of $\hat{\sigma}_x$. In all the presented states, there are negative values in the DV Wigner function. Importantly, in the DV Wigner function for qubits, negative volume, as well as being an indicator of non-classicality, is also a measure of purity [37]. This is because discrete system coherent states are fundamentally quantum; regardless of whether the system is the polarization of a photon or the direction of spin in an electron.

More generally, in both CV and DV Wigner functions, negative values arise as a consequence of self-interference. In the CV Wigner function this arises from non-Gaussianity [61], and can be seen in the Fock states

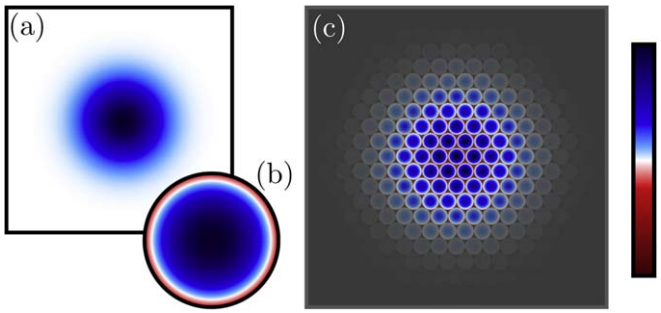

Figure 2. Example Wigner function for the product of the CV vacuum state and a DV excited state, $|0\rangle_f|\uparrow\rangle_a$, where (a) and (b) show the reduced Wigner functions for the continuous-variable (CV) and discrete-variable (DV) Wigner functions respectively. In (c) is the full Wigner function of the hybrid system, where the CV phase space is split up as a discrete grid. At each of these discrete points the DV Wigner function at that point in phase space is plotted. The transparency of each of the DV Wigner functions is proportional to the maximum quasi-probability at that point in CV phase space. The colour bar is white at 0 with limits ± 2 for (a), $\pm(1+\sqrt{3})/2$ for (b), and $\pm(1+\sqrt{3})$ for (c).

(excluding the vacuum state) or in superpositions of Gaussian states, see figure 3 for an example, discussed later in the paper. This explains why negative values have been used as a measure of quantumness, however there is one notable exception, the non-negative, entangled, Gaussian CV two-mode squeezed state.

Since the Gaussian states of a DV Wigner function can be visualized on a sphere, the emergence of self-interference is now inevitable, due to the inherent geometry of the sphere. For example, the Wigner function for the state $|\uparrow\rangle_a$ has a Gaussian distribution centred at the north pole; as this Gaussian distribution tends towards zero, near the south pole, there is an emergence of negative quasi-probabilities. This negativity in the Wigner function is manifested as a result of self-interference, as the quantum coherences interfere with each other at the south pole. As the number of levels is increased (from the two-level system) in the DV Wigner function and take the infinite limit[6], the $SU(2)$ DV Wigner function tends towards the Heisenberg-Weyl group, returning to the standard CV Wigner function. This is because the effective size of the sphere increases, decreasing the relative size of the Gaussian. In the infinite limit, the negativity in the Wigner function is completely eliminated, since the Gaussian can no longer interact with itself on the opposite side of the sphere.

Although the example states so far have been density operators for pure states, the general formalism in (1) allows for the Wigner function to be generated for any arbitrary operator. To emphasize this, in figures 1(d)–(f) are the DV Wigner representation of each of the three Pauli operators. In general, Wigner function exhibit the normalization condition

$$\int_{\Omega} \mathrm{d}\Omega\ W_{\hat{A}}(\Omega) = \mathrm{Tr}[\hat{A}]. \tag{7}$$

For normal density operators, this yields unity, as would be expected for any probability distribution function. For the Pauli operators however, $\mathrm{Tr}[\hat{\sigma}_i] = 0$, where $i = \{x, y, z\}$, therefore $\int_{\Omega} \mathrm{d}\Omega\ W_{\hat{\sigma}_i}(\Omega) = 0$. The tracelessness of these matrices can be seen in figures 1(d)–(f) by noting that the negative and positive volumes are equivalent and therefore cancel. This feature will be key to several of our observations later in this work.

For a CV-DV hybrid system, the total displaced parity operator is simply the tensor product of the displaced parity operator for each subsystem [23, 24, 28]

$$\hat{\Pi}(\alpha, \theta, \phi) = \hat{\Pi}_f(\alpha) \otimes \hat{\Pi}_a(\theta, \phi), \tag{8}$$

yielding a hybrid Wigner function for a density matrix $\hat{\rho}$

$$W_{\hat{\rho}}(\alpha, \theta, \phi) = \mathrm{Tr}[\hat{\rho}\ \hat{\Pi}(\alpha, \theta, \phi)]. \tag{9}$$

Hybrid systems generated with (9) usually have more degrees of freedom than is convenient to plot. For this reason, many approaches that use phase-space methods to treat hybrid systems use reduced Wigner functions, rather than considering the full phase space of the composite system. To give a full picture of the quantum correlations found between the two systems, a method similar to that introduced in [38] can be used. As an example of the utility of this method, the fully separable state, $|0\rangle_f|\uparrow\rangle_a$, is shown in figure 2. The reduced Wigner functions for CV and DV degrees of freedom are presented in figures 2(a) and (b) respectively. In figure 2(c) we apply the method first presented in [38] to plot the phase-space representation of this state.

Specifically, figure 2(c) was created by first dividing the CV phase space into discrete points on a rectangular map. Each of these discrete points is then associated with a discrete complex value α, equally spaced across the

[6] The general Wigner function for any system in the displaced parity formalism can be found in [24].

phase space grid. For each set point α, the values of the Wigner function for θ and ϕ degrees of freedom are calculated, with the Wigner function at that point plotted using the Lambert projection. This produces a DV Wigner function at each α in CV phase space. The transparency of each disc is then set proportional to the absolute maximal value of the phase space at that point, $\max_{\theta,\phi}|W_{\hat{\rho}}(\alpha,\ \theta,\ \phi)|$. For example, to generate the disc at the centre of figure 2(c), we calculate $W_{\hat{\rho}}(\alpha = 0,\ \theta,\ \phi)$, resulting in a DV Wigner function for $|\uparrow\rangle_a$, and then modify the amplitudes of the quasi-probabilities using the value of α. This is then repeated for every α. Note that a main difference between the plots presented here and in [38] is that the transparency of the DV Wigner functions in [38] is set proportional to $|W_f(\alpha)|$. Using the method presented here allows for a clearer view of the quantum correlations that manifest.

Since the state being plotted here is a pure separable state, the Wigner function can be expressed as

$$W_{\hat{\rho}}(\alpha,\ \theta,\ \phi) = W_{\hat{\rho}_f}(\alpha)\, W_{\hat{\rho}_a}(\theta,\ \phi), \tag{10}$$

where $\hat{\rho}_f$ and $\hat{\rho}_a$ are the reduced density matrices for the CV and DV systems respectively. As a result, figure 2(c) has the same form as a coherent state, dictated by the CV Wigner function, with every point in phase space having an $|\uparrow\rangle_a$ DV Wigner function. The difference in this method, in comparison to [38], is that here the transparency is not set by integrating out the qubit degrees of freedom; such an approach leads to a loss of quantum correlations in the systems of interest.

3. Visualizing correlations in hybrid quantum systems

Quantifying different types of correlations in quantum systems is a key area of research that has received a great deal of attention [62–69]. In parallel, phase-space methods have been utilized as a tool to identify and categorize quantum correlations [41, 70–73]. Further, these methods have been used to generate measures based on the emergence of negative quasi-probabilities in the Wigner function [37, 74–76]. However, due to the higher number of degrees of freedom, visually representing correlations in composite systems is more difficult. We now show how our technique produces definite signatures of both quantum and classical correlations, that can be discerned for hybrid quantum systems. When dealing with quantum information processing with two coupled qubits, the distinction between these two types of correlations is important. Beginning with how correlations that arise from superposition appear, we will describe our choices of DV and CV qubits and how the encoding of quantum information is represented on these qubits.

Certain similarities are seen between DV and CV systems, whether in structure, choice in qubit, or in appearance of the quantum correlations that manifest. These similarities will be demonstrated here, by showing how quantum information can be encoded onto different types of state. Encoding quantum information onto quantum states can be done in various ways, including a variety of approaches even within the same system [45]. We will therefore begin by using the simplest case of a DV qubit for quantum information processing. Since the DV systems used here are two-level systems, the encoding of quantum information is straightforward; a bit value 0 or 1 is simply assigned to each of the two levels, $|\uparrow\rangle_a$ and $|\downarrow\rangle_a$ respectively. The DV 0bit is now represented visually by figure 1(a), likewise the 1 bit value is represented by figure 1(b). Furthermore, a general pure superposition state

$$a_a\,|\uparrow\rangle_a + b_a\,|\downarrow\rangle_a, \tag{11}$$

where $|a_a|^2 + |b_a|^2 = 1$, allowing any weighted superposition between 0 and 1. When $a_a = b_a = 1/\sqrt{2}$, an equal superposition is yielded and is represented visually by figure 1(c).

This binary choice becomes more complicated when assigning bit values to a CV qubit. Although, there are various ways to encode quantum information onto a CV system creating similarities between CV and DV systems. Since the Hilbert space is infinite, there are different constraints on assigning qubit values. We will now demonstrate two examples of CV qubits, comparing the results with the DV qubits

3.1. Fock state qubits

Fock states are orthogonal and therefore a natural choice for quantum information processing. For simplicity we consider the vacuum and one-photon Fock states, $|0\rangle_f$ and $|1\rangle_f$ respectively. We can now form the analogy with the DV qubit state by assigning bit values to these states $0 \rightarrow |0\rangle_f$ and $1 \rightarrow |1\rangle_f$.

Comparison of the Wigner functions for the DV and the CV Fock qubits can be found in figures 2(a) and (b); where in the Lambert projection, the DV qubit in figure 2(b) has a similar Gaussian form as the vacuum state in figure 2(a). In fact, the DV qubit basis states are discrete analogues of the Fock states. Therefore, the presence of the negative values in the DV qubit states becomes more apparent by considering the one-photon Fock state $|1\rangle_f$ and the DV qubit state $|\downarrow\rangle_a$ (in figures 3(a) and (b) respectively). The orientation of the DV qubit is somewhat arbitrary, the $|\uparrow\rangle_a$ and $|\downarrow\rangle_a$ states are orthogonal rotations of one another; therefore, the DV qubit states share

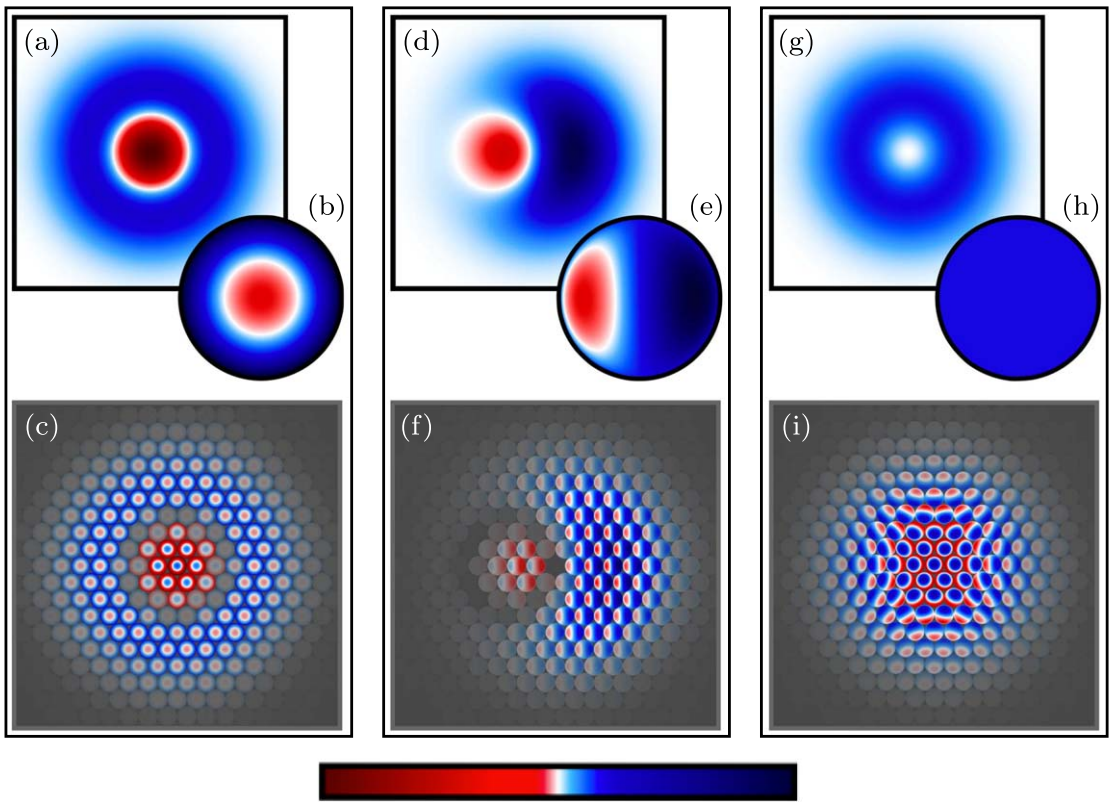

Figure 3. Examples of Fock states coupled to DV qubits. (a) - (c) show the state $|1\rangle_f|\downarrow\rangle_a$. (d)–(f) are the state $(|0\rangle_f + |1\rangle_f)(|\uparrow\rangle_a + |\downarrow\rangle_a)/2$. (g)–(i) are the entangled state $(|0\rangle_f|\uparrow\rangle_a + |1\rangle_f|\downarrow\rangle_a)/2$. (a), (d), and (g) show the reduced CV Wigner functions, (b), (e), and (h) are the reduced DV Wigner functions and (c), (f), and (i) are the full hybrid Wigner functions. The colour bar is white at 0 with limits ± 2 for the reduced CV Wigner function, $\pm(1+\sqrt{3})/2$ for reduced DV Wigner function, and $\pm(1+\sqrt{3})$ for hybrid Wigner function.

properties of both the $|0\rangle_f$ and $|1\rangle_f$ Fock states. This analogy can be seen further in figures 3(d) and (e), where the Wigner functions for the states $(|0\rangle_f + |1\rangle_f)/\sqrt{2}$ and $(|\uparrow\rangle_a + |\downarrow\rangle_a)/\sqrt{2}$ are shown respectively.

Also in figure 3, we show the hybrid Wigner functions for these states. In figure 3(c) we show the product of figures 3(a) and (b). The product of figures 3(d) and (e) is shown in figure 3(f). Since in both cases the CV and DV qubits are separable and therefore follow (10), the pattern of the hybrid phase space is similar to that found in figure 2. The separability is evident by the existence of a DV Wigner function at every point in CV phase space, with the amplitude modulated by the CV Wigner function at that point. For both of the hybrid Wigner functions in figures 3(c) and (f), the negative regions in the CV Wigner functions affect the sign of the DV Wigner function, causing there to be a negative prefactor whenever $W_{\hat{\rho}_f}(\alpha) < 0$, inverting the positive and negative quasi-probabilities at those points in CV phase space.

Having established that the hybrid Wigner function allows local correlations to be discerned reliably, we now demonstrate how quantum correlations arising between subsystems in this type of hybrid system manifest. Entanglement in Fock hybrid states, a Bell-Fock state[7], $(|0\rangle_f|\uparrow\rangle_a + |1\rangle_f|\downarrow\rangle_a)/\sqrt{2}$, is shown in figure 3(i). The full Wigner functions for bipartite Bell-Fock states have a distinctive pattern, reminiscent of the spin-orbit coupled state from [38], where there is a twisting of the DV Wigner functions dependent on the point in CV phase space. This DV dependence on the CV Wigner function is indicative that (10) does not hold for this state. This means that the state in question is not separable, and since this state is a pure state this indicates coupling between the two subsystems. This is a signature one should look for when investigating quantum correlations in this type of hybrid state.

Comparing the hybrid Wigner function in figure 3(i) to the reduced Wigner function for the CV and DV qubits in figures 3(g) and (h) respectively, we see the importance in considering the full phase space for entangled states such as this. It can be seen in figures 3(g) and (h) how correlations between the two systems are lost when considering the reduced Wigner functions, leaving only statistical mixtures of the basis states in each case.

[7] Bell state for an entangled DV qubit with a CV Fock qubit.

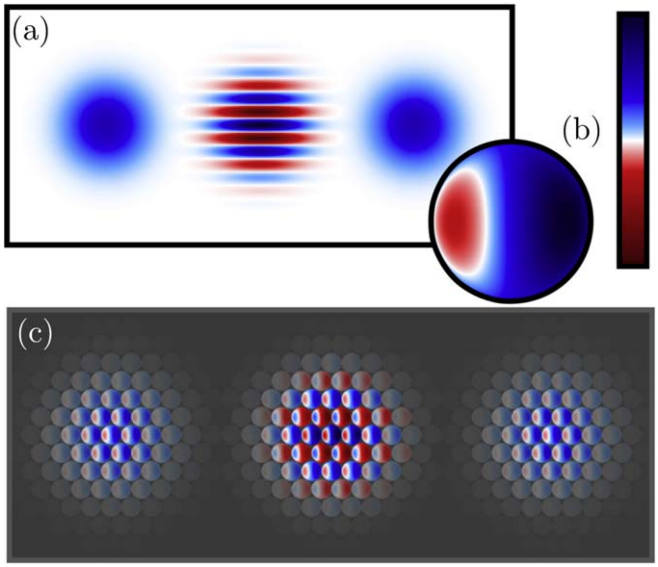

Figure 4. Here is an example of the Wigner representation of a Schrödinger cat state coupled to a qubit, $(|\beta\rangle_f + |-\beta\rangle_f)(|\uparrow\rangle_a + |\downarrow\rangle_a)/2$, where $|\beta\rangle$ is a coherent state centred at β for $\beta = 3$. (a) shows the reduced CV Wigner function and (b) shows the reduced DV Wigner function. (c) shows the hybrid Wigner function. The colour bar is white at 0 with limits ± 2 for (a), $\pm(1 + \sqrt{3})/2$ for (b), and $\pm(1 + \sqrt{3})$ for (c).

3.2. Coherent state qubits

Another choice in creating a CV qubit is to encode quantum information onto coherent states [5, 6]. Unlike with the Fock CV qubit, the coherent state basis is an overcomplete basis where there is some degree of overlap between any two coherent states. However with sufficient distance between two coherent states, this overlap is negligible. For simplicity, our example states will be real values of β, where the two levels are set to the values $\beta_1 = -\beta_2 = \beta$.

We then label each of the coherent states as a certain bit value; for instance $0 \rightarrow \beta_1$ and $1 \rightarrow \beta_2$. This creates a qubit in the form of a Schrödinger cat state [6], with the general qubit state being

$$a_f\,|\beta\rangle_f + b_f\,|-\beta\rangle_f, \tag{12}$$

as in (11). This means that there is a coherent state at β when $a_f = 1$ and a coherent state at $-\beta$ when $b_f = 1$. The superposition state $a_f = b_f = 1/\sqrt{2}$ produces the Schrödinger cat state shown (for $\beta = 3$) in figure 4(a).

Coupling the CV and DV qubits in figgures 4(a) and (b) generates the full Wigner function in figure 4(c). Explicitly, this is the state

$$\frac{1}{2}(|\beta\rangle_f + |-\beta\rangle_f)(|\uparrow\rangle_a + |\downarrow\rangle_a). \tag{13}$$

Since the full system is a simple tensor product of the two qubits, the subsystems are separable, resulting in a full Wigner function that obeys (10). The separability between these states is seen in the full Wigner function in figure 4(c). The image of the CV Schrödinger cat state is visible as a discrete grid, with the DV Wigner function for the state at every point.

Given the difference in the local correlations between the two choices of CV qubit, it is now worthwhile to demonstrate how the signature of the non-local correlations differ for the coherent state CV qubits. The hybrid analogue of a Bell state for coherent states, the Bell-cat state, is

$$\frac{1}{\sqrt{2}}(|\beta\rangle_f|\uparrow\rangle_a + |-\beta\rangle_f|\downarrow\rangle_a). \tag{14}$$

Since many of the correlations in this state are due to entanglement, the standard approach of using reduced Wigner functions is insufficient, as seen in figures 5(a) and (b). Neither reduced Wigner function has visible quantum correlations, yielding two mixed states. This issue motivated other approaches to tomography and state verification for such states, for instance [40] used reduced CV Wigner functions in different Pauli bases to show Bell's inequality. Other tomography methods for entangled hybrid systems, such as [47], also take into consideration the problems of a reduced phase-space representation of a hybrid entangled state. Although approaches such as these give a better appreciation of the quantum correlations, they still only provide glimpses of the nature of the full quantum state.

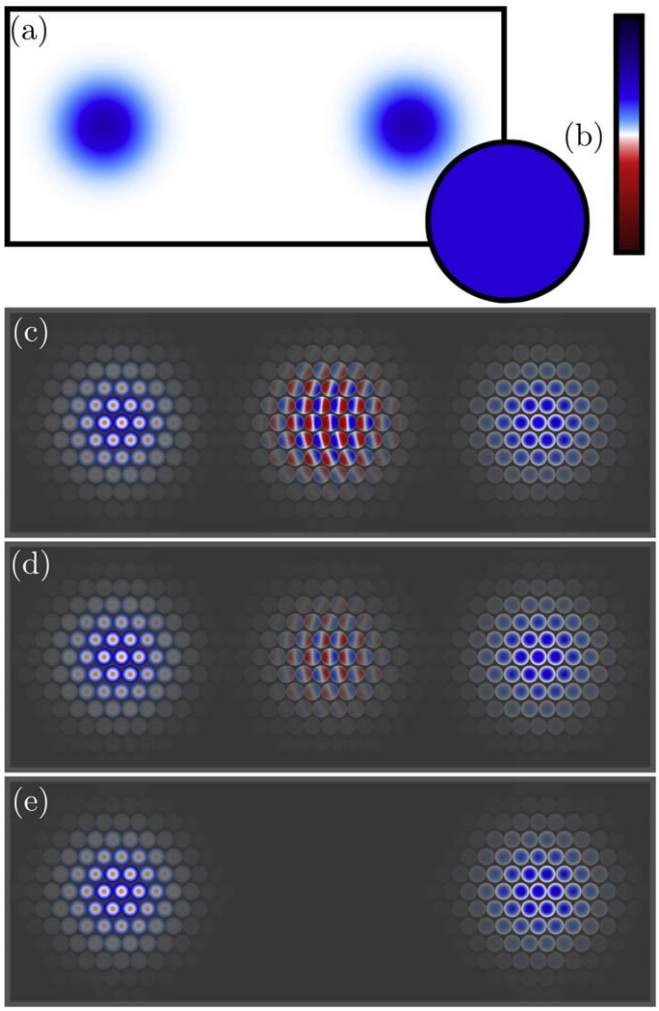

Figure 5. Here are examples of the Wigner representation of a lossy entangled Bell-cat state, with varying values of loss. (a) shows the reduced CV Wigner function and (b) shows the reduced DV Wigner function. The reduced Wigner functions remain the same for the following three example states. (c) shows the full Wigner function for the state with no loss $(|\alpha\rangle_f|\uparrow\rangle_a + |-\alpha\rangle_f|\downarrow\rangle_a)/\sqrt{2}$. (d) shows partial loss of the quantum correlations. (e) shows a fully mixed version of the state $(|\beta\rangle\langle\beta|_f|e\rangle\langle e|_a + |-\beta\rangle\langle-\beta|_f|g\rangle\langle g|_a)/2$. The colour bar is white at 0 with limits ± 2 for (a), $\pm(1+\sqrt{3})/2$ for (b), and $\pm(1+\sqrt{3})$ for (c).

The hybrid Wigner function for (14) is shown in figure 5(c). Comparing our representation with the reduced Wigner function treatment, the quantum correlations are now visible, manifesting as interference terms between the two coherent states. The nature of these quantum correlations is completely lost when the full Wigner function is not generated. Further, within the quantum correlations, the qubit states approach traceless states, as in figures 1(d)–(f), where the state at the very centre, $\alpha = 0$, is in fact the $\hat{\sigma}_x$ Pauli matrix. It is important to note at this point that the manifestation of traceless here, found only in the hybrid phase-space picture, are a signature of quantum correlations. Some existing tomography methods can pick up these correlations, however their full nature is not captured. For example, measuring the reduced Wigner functions results in a loss of quantum and classical correlations, as demonstrated in figures 5(a) and (b). This makes classical and quantum correlations, for this kind of state, indistinguishable. The ability to obtain signatures to distinguish between classical and quantum correlations is important in determining the suitability of states in quantum information processing.

To highlight this, we now consider two further examples of states that have the same reduced CV and DV Wigner functions. Though the degree of quantum correlations differ for each state. The general state is

$$\frac{1}{2}(|\beta\rangle\langle\beta|_f|e\rangle\langle e|_a + \eta|\beta\rangle\langle-\beta|_f|e\rangle\langle g|_a + \eta|-\beta\rangle\langle\beta|_f|g\rangle\langle e|_a + |-\beta\rangle\langle-\beta|_f|g\rangle\langle g|_a), \tag{15}$$

where η determines the purity of the state. When $\eta = 1$ (15) reduces to (14). Changing the value of the loss to $\eta = 0.5$ and then to $\eta = 0$, figures 5(d) and (e) are, respectively, generated. In both, it is clear that the quantum correlations are slowly lost. The loss of quantum correlations means these states are less useful for quantum information purposes, and analyzing the reduced Wigner functions, unlike our approach, does not provide any

insight to this loss. By using our method to represent the full Wigner function, it is not only possible to distinguish the strength of the quantum correlations but, the signature of classical correlations is revealed.

In figure 5(e) is the state

$$\frac{1}{2}(|\beta\rangle\langle\beta|_f|e\rangle\langle e|_a + |-\beta\rangle\langle-\beta|_f|g\rangle\langle g|_a) \tag{16}$$

that describes the equal classical probability of finding an excited state at β and a ground state at $-\beta$. The classical correlations that correspond to this probability is shown in our full picture of the Wigner function, where the $|\beta\rangle_f$ coherent state is correlated with $|\uparrow\rangle_a$ states, likewise the $|-\beta\rangle_f$ coherent state is correlated with $|\downarrow\rangle_a$ states. This process not only reveals that this is the signature of classical correlations, it verifies the case that the traceless states between the two states are a result of the quantum correlations within the hybrid system.

4. The Jaynes-Cummings model

Light-matter interaction in the form of quantum electrodynamics (QED) has been an experimental cornerstone in understanding quantum effects. It has also given a helping hand in the development of quantum information applications, such as single-photon quantum non-demolition measurements acting as two-qubit gates between microwaves and atoms [35]. The standard example of a QED interaction between a two-level DV system and a CV field is the Jaynes–Cummings model [36]. Jaynes–Cummings type interactions are the basis for the generation of non-Gaussian states and are well known for showing the collapse and revival of Rabi oscillations [66, 77, 78] throughout its evolution. During this evolution, quantum information is transferred back and forth between the CV and DV systems; through this process, quantum information can then manifest as a Schrödinger cat state or generate Bell pairs of the sort shown in figure 3(i). By using our methods, the transfer of quantum information can be visualized as is swaps between the microwave field and the atom.

The interaction picture of the Jaynes–Cummings model

$$\hat{H}_{\rm JC} = \omega(\hat{a}^\dagger\hat{\sigma}_- + \hat{a}\hat{\sigma}_+), \tag{17}$$

will be used, where ω is the field-qubit coupling constant, and the operators $\hat{\sigma}_\pm = (\hat{\sigma}_x \pm i\hat{\sigma}_y)/2$ are the qubit raising and lowering operators that transition the state between eigenstates of $\hat{\sigma}_z$.

Following the example given in section 3, we consider a Fock state basis to model the Jaynes-Cumming model. Choosing the initial state in the field to be a vacuum state and coupling it to an excited DV qubit results in an evolution that fluctuates between $|0\rangle_f|\uparrow\rangle_a$ and $|1\rangle_f|\downarrow\rangle_a$ [35], as shown in figures 2 and 3(d)–(g) respectively. This means that the evolution can be fully described with the two levels of the Fock state qubit and the DV qubit, allowing us to consider this as an exchange between two qubits.

The fluctuation as part of this model results in the system continuously transferring quantum information between the two qubits, where the state at time t is

$$|\Psi(t)\rangle = \cos(\omega t)|0\rangle_f|\uparrow\rangle_a - i\sin(\omega t)|1\rangle_f|\downarrow\rangle_a, \tag{18}$$

returning to the initial state at $t = \pi/\omega$. A video of this evolution is given in supplementary material. As the information transfers between these two states, throughout one period, two entangled Bell-Fock states are generated

$$|\Phi^\pm\rangle = \frac{1}{\sqrt{2}}(|0\rangle_f|\uparrow\rangle_a \pm i\,|1\rangle_f|\downarrow\rangle_a), \tag{19}$$

where the full Wigner functions for these states are shown in figure 6. Both of these states have the same reduced Wigner functions, which are not shown here since all Bell-Fock states have the same reduced Wigner functions, shown in figures 3(g) and (h).

During Jaynes–Cummings evolution, the first of the Bell-Fock states appears at $t = \omega^{-1}\pi/4$, where the state $|\Psi(\omega^{-1}\pi/4)\rangle = |\Phi^-\rangle$. This first Bell-Fock state is shown in figure 6(a), the second $|\Psi(3\omega^{-1}\pi/4)\rangle = |\Phi^+\rangle$ is given in figure 6(b). Comparing these two states to figure 3(i), even though the reduced Wigner functions are identical, the difference the phase plays in the full hybrid Wigner functions is apparent. Extrapolating to another choice of phase, for example $(|0\rangle_f|\uparrow\rangle_a - |1\rangle_f|\downarrow\rangle_a)/\sqrt{2}$, the full hybrid Wigner function is similar to figure 3(i) with each of the DV Wigner functions pointing in the orthogonal directions. The quantum correlations that arise in this form of hybrid system have a unique signature which can best be described as a twisting of the DV Wigner function at points in CV phase space.

We now consider the JCM evolution with a different initial state. The vacuum state is replaced by a coherent state, giving the initial state $|\beta\rangle_f|\uparrow\rangle_a$, where again $\beta = 3$. This choice of initial state produces very different effects in the Jaynes-Cumming model, such as the collapse and revival of the Rabi oscillations, where the revival of the Rabi oscillations happen at time t_r. Three noteworthy snapshots, points within the evolution, of the Jaynes–Cummings model are shown in figure 7, indicated by the three vertical lines in figure 7(a), showing the value of

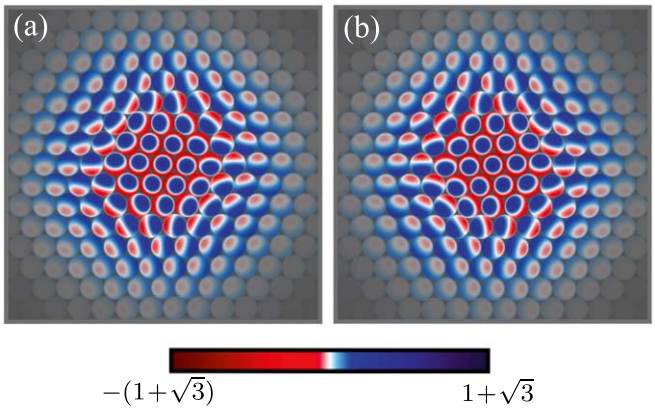

Figure 6. Here we show the Wigner functions for two points in the evolution of the Jaynes–Cummings model with initial state $|0\rangle_f|\uparrow\rangle_a$. During the evolution of the Jaynes–Cummings model with this excited state, two entangled Bell-Fock states are generates before returning to the initial state again. The two entangled Fock-States are shown here, where the first one in (a) is the state $(|0\rangle_f|\uparrow\rangle_a - \mathrm{i}\,|1\rangle_f|\downarrow\rangle_a)/\sqrt{2}$. The second entangled Bell-Fock state in the evolution is shown in (b), where the state is $(|0\rangle_f|\uparrow\rangle_a + \mathrm{i}\,|1\rangle_f|\downarrow\rangle_a)/\sqrt{2}$. The signature of entanglement in these states can be seen in the DV Wigner function dependence on the value of the CV Wigner function, similarly to the example state in figure 3(i).

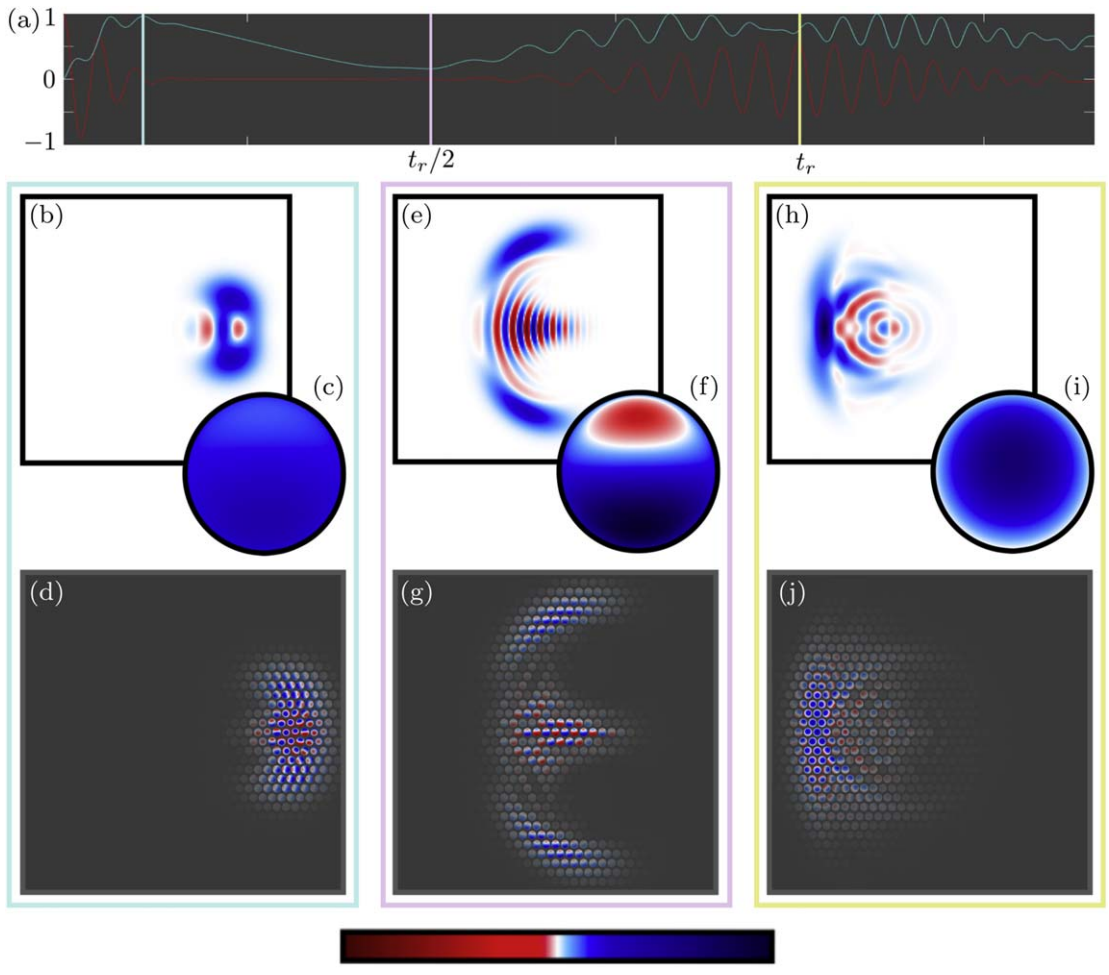

Figure 7. Here we show the Wigner functions for three points in the evolution of the Jaynes–Cummings model with initial state $|\beta\rangle_f|\uparrow\rangle_a$, where $\beta = 3$. (a) shows the qubit inversion, $\langle\hat{\sigma}_z\rangle$, in red and the von Neumann entropy in cyan over time. t_r is the revival time of the Rabi oscillations. Three solid lines are shown in (a) that indicate the different point in the evolution where we have displayed the Wigner functions. The reduced Wigner functions are then given below (a), where the reduced CV Wigner functions are in (b), (e), and (h). The reduced DV Wigner functions are in (c), (f), and (i). The hybrid Wigner functions for the coupled system are in (d), (g), and (j). The values for the colours correspond to the same values in figures 4 and 5.

the von Neumann entropy (cyan) and qubit inversion, $\langle\hat{\sigma}_z\rangle$, (red) at each point in the evolution. For each of the snapshots the reduced Wigner functions are figures 7(b), (e), and (h) for the CV system, and figures 7(c), (f), and (i) for the DV qubit. In figures 7(d), (g), and (j) are the full Wigner function for each of these snapshots.

The first snapshot is early on in the evolution, $t \approx t_r/9$, where there is a high degree of coupling between the two systems. The reduced Wigner functions in figures 7(b) and (c), indicate that something approaching a Schrödinger cat state forming in the CV system; where the DV qubit is in a highly mixed state. All that can be deduced from the reduced Wigner functions then is that there are correlations between the qubit and the field mode; the nature of the quantum correlations remains hidden.

Evaluating the full Wigner function in figure 7(d), a better appreciation of the quantum correlations at this point in the evolution can be obtained. The DV spin direction at the top of the CV Wigner functions are orthogonal to those in the bottom of the CV Wigner function. Where at the top, the spins point in the direction of the negative eigenstate of $\hat{\sigma}_x$; at the bottom they point in the positive eigenstate of $\hat{\sigma}_x$. The correlations found in the middle in figure 7(d) match the quantum correlation signature for a coherent state qubit, as they are of a form similar to the traceless states in figure 1.

The second snapshot of the Jaynes–Cummings model, $t \approx t_r/2$, is where the field mode and the qubit disentangle, transferring the quantum correlations to form a CV Schrödinger cat state. Presence of this Schrödinger cat state is immediately visible in the reduced CV Wigner function in figure 7(e). The reduced DV Wigner function in figure 7(f) has now increased in both negative and positive amplitudes, rotating to the eigenstate of $\hat{\sigma}_y$ with eigenvalue -1. The return of coherence of the DV qubit is a good indication that the correlations between the two systems have decreased.

Both of the reduced Wigner functions in figures 7(e) and (f) suggest that this state is similar to the example state in figure 4, which is approximately separable. Observation of figure 7(g) confirms this suggestion, but more detail can still be found. Although very few correlations appear between the two subsystems, some residual quantum correlation has remained between the two. These correlations are found in the slight twisting of the qubits around the two cats and within the quantum correlations in between.

The final snapshot occurs at the revival of the Rabi oscillations, $t \approx t_r$, where the qubit state is closest to the initial state within the revival. In figure 7(i) the average spin is pointing in the direction of an excited state $|\uparrow\rangle_a$, however, there is a loss of coherence associated with the decrease in amplitudes and no negative values. The full Wigner function reveals why the coherences in the reduced DV Wigner function have formed. At most points in the full Wigner function, the DV Wigner function is in the excited state, however at many points there are rotations in the qubit Wigner functions, indicating some residual quantum correlations. The strongest coherent states are found on the left-hand side, where it appears the state is returning to the initial state of a coherent state coupled to $|\uparrow\rangle_a$.

The quantum correlations that accompany the two choices of CV qubits have a somewhat different nature however their signatures are distinguishable when considering the full Wigner function. The correlations for the Fock state qubits show a dependence on each other, arising due to the non-separability of the state. This closely resembles the pattern found in spin-orbit coupled states [38], and is comparable to spin texture images. The fundamental signatures come from the behaviour of the coherences and correlations within and between the systems. The form of the Wigner function of a two-mode squeezed state, although lacking negative values due to it being Gaussian, resembles the signature identified for the Bell-Fock states; the spatial dependence of one system affecting the state in the other system.

5. Conclusions

By plotting the information generated by calculating the Wigner function for a CV-DV hybrid system, we have shown that the usual techniques for visualizing these systems misses the full nature of the quantum correlations that arise. For example, the most common technique of generating the reduced Wigner function causes the correlations that arise between the systems to be traced out. Tracing out a system results in a loss of correlations that can be found between the two systems. A method to overcome this loss of information was presented in [38], but an envelope was applied setting the transparency of the points in phase space according to the reduced Wigner function for the CV degrees of freedom $W_f(\alpha)$. Here this method has been developed, changing the envelope to instead be proportional to $\max_{\theta,\phi}|W_{\hat{\rho}}(\alpha,\,\theta,\,\phi)|$ at each point in CV phase space. This adjustment further allows us to visualize the quantum correlations present in CV-DV hybrid states, such as those that manifest between the two coherent states in a hybrid Schrödinger cat state. Doing this means it is possible to gain a more full picture of the correlations that arise in the interaction between CV and DV systems. As well as allowing us to characterize signatures of quantum correlations found in certain systems; a result that promises potential usefulness in analyzing the correlations in maximally entangled states and entanglement as a result of squeezing. Being able to visually determine the level of quantum correlations, not always clear in coupled

systems, gives significant advantage over reduced Wigner function methods that do not always detect the purity of Bell-cat like entanglement.

By demonstrating these methods within the Jaynes–Cummings model, we show how excitations are shared and swapped, demonstrating a visual representation of the transfer of quantum information between systems. Extending these methods to different systems, will allow for a more intuitive picture of how quantum information moved around coupled systems, providing further insight into the inner process of quantum processes and algorithms.

There have been previous experimental examples which have used phase space to investigate the types of state considered in this paper. One notable example is [47], from a sequence of measurements of the expectation values of the qubit in different bases, they have been able to recreate the CV Wigner function. Using a similar procedure with our generalized displaced parity operator, it should be possible to extend this to produce experimental results equivalent to those in this paper. This technique could be considered to be a form of quantum state spectroscopy.

Acknowledgments

RPR is funded by the EPSRC [grant number EP/N509516/1]. TT notes that this work was supported in part by JSPS KAKENHI (C) Grant Number JP17K05569. The authors would like to thank Kae Nemoto, William Munro and T D Clark for interesting and informative discussions.

ORCID iDs

M J Everitt https://orcid.org/0000-0002-4542-3918

References

[1] Wheeler J A and Zurek W H 1983 *Quantum Theory and Measurement* (Princeton, NJ: Princeton University Press))
[2] Nielson M A and Chuang I L 2000 *Quantum Computation and Quantum Information* (Cambridge: Cambridge University Press))
[3] Wiseman H M and Milburn G J 2009 *Quantum Measurement and Control* (Cambridge: Cambridge University Press))
[4] Gerry C and Knight P L 2005 *Introductory Quantum Optics* (Cambridge: Cambridge University Press))
[5] Ralph T C, Gilchrist A, Milburn G J, Munro W J and Glancy S 2003 Quantum computation with optical coherent states *Phys. Rev.* A **68** 042319
[6] Gilchrist A, Nemoto K, Munro W J, Ralph T C, Glancy S, Braunstein S L and Milburn G J 2004 Schrödinger cats and their power for quantum information processing *J. Opt.* B **6** S828–33
[7] Braunstein S L and van Loock P 2005 Quantum information with continuous variables *Rev. Mod. Phys.* **77** 513–77
[8] Neergaard-Nielsen J S, Takeuchi M, Wakui K, Takahashi H, Hayasaka K, Takeoka M and Sasaki M 2010 Optical continuous-variable qubit *Phys. Rev. Lett.* **105** 1–4
[9] Hillery M, O'Connell R F, Scully M O and Wigner E P 1984 Distribution functions in physics: Fundamentals *Phys. Rep.* **106** 121
[10] Scully M O and Zubairy M S 2006 *Quantum Optics* 5 edn. (Cambridge: Cambridge University Press))
[11] Breitenbach G, Schiller S and Mlynek J 1997 Measurement of the quantum states of squeezed light *Nature* **387** 471–5
[12] Brune M, Haroche S, Raimond J M, Davidovich L and Zagury N 1992 Manipulation of photons in a cavity by dispersive atom-field coupling: Quantum-nondemolition measurements and generation of Schrödinger cat states *Phys. Rev.* A **45** 5193–214
[13] Schumacher B 1995 Quantum coding *Phys. Rev.* A **51** 2738–47
[14] Ladd T D, Jelezko F, Laflamme R, Nakamura Y, Monroe C and O'Brien J L 2010 Quantum computing *Nature* **464** 45–53
[15] Wootters W K 1987 A wigner-function formulation of finite-state quantum mechanics *Ann. Phys. (N.Y.)* **176** 1–21
[16] Gibbons K S, Hoffman M J and Wootters W K 2004 Discrete phase space based on finite fields *Phys. Rev.* A **70** 062101
[17] Howard M, Wallman J, Veitch V and Emerson J 2014 Contextuality supplies the 'magic' for quantum computation *Nature* **510** 351–5
[18] Delfosse N, Guerin P A, Bian J and Raussendorf R 2015 Wigner function negativity and contextuality in quantum computation on rebits *Phys. Rev.* X **5** 021003
[19] Raussendorf R, Browne D E, Delfosse N, Okay C and Bermejo-Vega J 2017 Contextuality and Wigner-function negativity in qubit quantum computation *Phys. Rev.* A **95** 1–22
[20] Dowling J P, Agarwal G S and Schleich W P 1994 Wigner distribution of a general angular-momentum state: Applications to a collection of two-level atoms *Phys. Rev.* A **49** 4101
[21] Várilly J C and Gracia-Bondía J M 1989 The moyal representation for spin *Ann. Phys. (N.Y.)* **190** 107–48
[22] Brif C and Mann A 1999 Phase-space formulation of quantum mechanics and quantum-state reconstruction for physical systems with lie-group symmetries *Phys. Rev.* A **59** 971–87
[23] Tilma T, Everitt M J, Samson J H, Munro W J and Nemoto K 2016 Wigner functions for arbitrary quantum systems *Phys. Rev. Lett.* **117** 180401
[24] Rundle R P, Tilma T, Samson J H, Dwyer V M, Bishop R F and Everitt M J 2019 General approach to quantum mechanics as a statistical theory *Phys. Rev.* A **99** 012115
[25] Klimov A B and Romero J L 2008 A generalized wigner function for quantum systems with the su (2) dynamical symmetry group *J. Phys. A.: Math. Theor.* **41** 055303
[26] Garon A, Zeier R and Glaser S J 2015 Visualizing operators of coupled spin systems *Phys. Rev.* A **91** 1–28
[27] Mukherjee R, Mirasola A E, Hollingsworth J, White I G and Hazzard K R A 2018 Geometric representation of spin correlations and applications to ultracold systems *Phys. Rev.* A **97** 1–13

[28] Rundle R P, Mills P W, Tilma T, Samson J H and Everitt M J 2017 Simple procedure for phase-space measurement and entanglement validation *Phys. Rev.* A **96** 022117
[29] Leiner D, Zeier R and Glaser S J 2017 Wigner tomography of multispin quantum states *Phys. Rev.* A **96** 1–14
[30] Tian Y, Wang Z, Zhang P, Li G, Li J and Zhang T 2018 Measurement of complete and continuous Wigner functions for discrete atomic systems *Phys. Rev.* A **013840** 1–6
[31] Chen B, Geng J, Zhou F, Song L, Shen H and Xu N 2019 Quantum state tomography of a single electron spin in diamond with wigner function reconstruction *Appl. Phys. Lett.* **114** 041102
[32] Song C *et al* 2019 Generation of multicomponent atomic schrödinger cat states of up to 20 qubits *Science* **365** 574–7
[33] Reiserer A, Kalb N, Rempe G and Ritter S 2014 A quantum gate between a flying optical photon and a single trapped atom *Nature* **508** 237–40
[34] Hacker B, Welte S, Daiss S, Shaukat A, Ritter S, Li L and Rempe G 2019 Deterministic creation of entangled atom–light Schrödinger-cat states *Nat. Photonics* **13** 110–5
[35] Haroche S and Raimond J M 2006 *Exploring the Quantum: Atoms, Cavities, and Photons.* (Oxford: Oxford Univ. Press))
[36] Jaynes E T and Cummings F W 1963 Comparison of quantum and semiclassical radiation theories with application to the beam maser *Proc. IEEE* **51** 89–109
[37] Arkhipov I I, Barasiński A and Svozilík J 2018 Negativity volume of the generalized Wigner function as an entanglement witness for hybrid bipartite states *Sci. Rep.* **8** 16955
[38] Davies B I, Rundle R P, Dwyer V M, Samson J H, Todd Tilma and Everitt M J 2018 Visualising entanglement in atoms *Phys. Rev.* A **100** 042102
[39] Jeong H, Zavatta A, Kang M, Lee S-W, Costanzo L S, Grandi S, Ralph T C and Bellini M 2014 Generation of hybrid entanglement of light *Nat. Photonics* **8** 564
[40] Vlastakis B *et al* 2015 Characterizing entanglement of an artificial atom and a cavity cat state with Bell's inequality *Nat. Commun.* **6** 1–8
[41] Sperling J, Agudelo E, Walmsley I A and Vogel W 2017 Quantum correlations in composite systems *J. Phys.* B **50** 134003
[42] Monroe C, Meekhof D M, King B E and Wineland D J 1996 A schrödinger cat superposition state of an atom *Science* **272** 1131–6
[43] Brune M, Hagley E, Dreyer J, Maître X, Maali A, Wunderlich C, Raimond J M and Haroche S 1996 Observing the progressive decoherence of the 'meter' in a quantum measurement *Phys. Rev. Lett.* **77** 4887–90
[44] Deléglise S, Dotsenko I, Sayrin C, Bernu J, Brune M, Raimond J M and Haroche S 2008 Reconstruction of non-classical cavity field states with snapshots of their decoherence *Nature* **455** 510–4
[45] Andersen U L, Neergaard-Nielsen J S, Van Loock P and Furusawa A 2015 Hybrid discrete- and continuous-variable quantum information *Nat. Phys.* **11** 713–9
[46] Morin O, Huang K, Liu J, Le Jeannic H, Fabre C and Laurat J 2014 Remote creation of hybrid entanglement between particle-like and wave-like optical qubits *Nat. Photonics* **8** 570
[47] Eichler C, Lang C, Fink J M, Govenius J, Filipp S and Wallraff A 2012 Observation of entanglement between itinerant microwave photons and a superconducting qubit *Phys. Rev. Lett.* **109** 240501
[48] Gottesman D, Kitaev A and Preskill J 2001 Encoding a qubit in an oscillator *Physical Review A. Atomic, Molecular, and Optical Physics* **64** 123101123101–21
[49] Lee N, Benichi H, Takeno Y, Takeda S, Webb J, Huntington E and Furusawa A 2011 Teleportation of nonclassical wave packets of light *Science* **332** 330–3
[50] Andersen U L and Ralph T C 2013 High-fidelity teleportation of continuous-variable quantum states using delocalized single photons *Phys. Rev. Lett.* **111** 1–5
[51] Takeda S, Mizuta T, Fuwa M, Van Loock P and Furusawa A 2013 Deterministic quantum teleportation of photonic quantum bits by a hybrid technique *Nature* **500** 315–8
[52] Van Loock P, Ladd T D, Sanaka K, Yamaguchi F, Nemoto K, Munro W J and Yamamoto Y 2006 Hybrid quantum repeater using bright coherent light *Phys. Rev. Lett.* **96** 1–4
[53] Ourjoumtsev A, Dantan A, Tualle-Brouri R and Grangier P 2007 Increasing entanglement between Gaussian states by coherent photon subtraction *Phys. Rev. Lett.* **98** 1–4
[54] Datta A, Zhang L, Nunn J, Langford N K, Feito A, Plenio M B and Walmsley I A 2012 Compact continuous-variable entanglement distillation *Phys. Rev. Lett.* **108** 1–5
[55] Wigner E P 1932 On the quantum correction for thermodynamic equilibrium *Phys. Rev.* **40** 749
[56] Groenewold H J 1946 On the principles of elementary quantum mechanics *Physica* **12** 405–60
[57] Cahill K E and Glauber R J 1969 Density operators and quasiprobability distributions *Phys. Rev.* **177** 1882
[58] Stratonovich R L 1956 On distributions in representation space *Sov. Phys—JETP* **31** 1012
[59] Everitt M J, Munro W J and Spiller T P 2012 Overcoming decoherence in the collapse and revival of spin schrödinger-cat states *Phys. Rev.* A **85** 022113
[60] Lambert J H 1772 *Beiträge zum gebrauch der mathematik und deren anwendungen* (Berlin: Verlag der Buchhandlung der Relschule)
[61] Hudson R L 1974 When is the wigner quasi-probability density non-negative? *Rep. Math. Phys.* **6** 249–52
[62] Bennett C H, DiVincenzo D P, Smolin J A and Wootters W K 1996 Mixed-state entanglement and quantum error correction *Phys. Rev.* A **54** 3824–51
[63] Vedral V, Plenio M B, Rippin M A and Knight P L 1997 Quantifying entanglement *Phys. Rev. Lett.* **78** 2275–9
[64] Wootters W K 1998 Entanglement of formation of an arbitrary state of two qubits *Phys. Rev. Lett.* **80** 2245–8
[65] Vedral V and Plenio M B 1998 Entanglement measures and purification procedures *Phys. Rev.* A **57** 1619–33
[66] Narozhny N B, Sanchez-Mondragon J J and Eberly J H 1981 Coherence versus incoherence: Collapse and revival in a simple quantum model *Phys. Rev.* A **23** 236–47
[67] Eisert J and Plenio M B 1999 A comparison of entanglement measures *J. Mod. Opt.* **46** 145–54
[68] Henderson L and Vedral V 2001 Classical, quantum and total correlations *J. Phys. A. : Math. Gen.* **34** 6899–905
[69] Adesso G, Bromley T R and Cianciaruso M 2016 Measures and applications of quantum correlations *J. Phys. A.: Math. Theor.* **49** 1–82
[70] Wallentowitz S, de Matos Filho R L and Vogel W 1997 Determination of entangled quantum states of a trapped atom *Phys. Rev.* A **56** 1205–11
[71] Agudelo E, Sperling J, Costanzo L S, Bellini M, Zavatta A and Vogel W 2017 Conditional hybrid nonclassicality *Phys. Rev. Lett.* **119** 1–6
[72] Sperling J and Walmsley I A 2018 Quasiprobability representation of quantum coherence *Phys. Rev.* A **062327** 1–14
[73] Sundar B, Wang K C and Hazzard K R A 2019 Analysis of continuous and discrete Wigner approximations for spin dynamics *Phys. Rev.* A **99** 43627
[74] Kenfack A and Zyczkowski K 2004 Negativity of the wigner function as an indicator of non-classicality *J. Opt. B: Quant. Semi. Opt.* **6** 396

[75] Taghiabadi R, Akhtarshenas S J and Sarbishaei M 2016 Revealing quantum correlation by negativity of the Wigner function *Quant. Inf. Process.* **15** 1999–2020
[76] Siyouri F, El Baz M and Hassouni Y 2016 The negativity of Wigner function as a measure of quantum correlations *Quant. Inf. Process.* **15** 4237–52
[77] Cummings F W 1965 Stimulated emission of radiation in a single mode *Phys. Rev.* **140** A1051–6
[78] Eberly J H, Narozhny N B and Sanchez-Mondragon J J 1980 Periodic spontaneous collapse and revival in a simple quantum model *Phys. Rev. Lett.* **44** 1323–6